FDTD Study on the Invisibility Performance of Two-Dimensional Cylindrical Cloak With Off-Plane Incidence

Xu-Lin Zhang, Jun-Feng Song, Xian-Bin Li, and Hong-Bo Sun, *Member, IEEE*

Abstract—In this paper, we derive a theory for the modeling of 3-D cylindrical cloak based on 2-D finite-difference time-domain method, which is less time consuming and memory saving. By using the method, we develop the concept of invisibility angle and investigate the invisibility performance of the 3-D cylindrical cloak with 2-D constitutive parameters under off-plane incident waves. The bistatic radar cross sections as well as the scattered fields are calculated to evaluate the scatterings, from which the invisibility performance is observed to get worse with the increase in the incident angle, while the defined invisibility angle diminishes with the decrease in the cloak thickness and wavelength. The deterioration of the invisibility performance is mainly caused by the scatterings of TM_2 wave defined in the study. The present results point out a possible way to evaluate the 2-D cloak on 3-D applications.

Index Terms—Cylindrical cloak, finite-difference time-domain (FDTD), invisibility performance, scatterings.

I. INTRODUCTION

RECENTLY, the development of transformation optics [1]–[3] has been making people's dreams of being invisible become more and more feasible. Based on the invariance of Maxwell's equations during the coordinate transformations, transformation optics can be used to design unique devices such as invisibility cloaks [4]–[9]. Cylindrical invisibility cloak is one of the most remarkable cloaks, which has attracted much attention, both theoretically and experimentally. It was first theoretically demonstrated by Pendry *et al.* [1] using a linear coordinate transformation, where the cloak bends and guides incident waves smoothly in the cloak region. Although the object in the cloak can be hidden perfectly, the material is required to have the permittivity and permeability with spatial inhomogeneity and anisotropy, which cannot be achieved by natural materials. Fortunately, with the help of the artificial metamaterials, the first cylindrical cloak was realized by

Schurig *et al.* [4] at microwave frequencies. In their experiment, the material properties were simplified and only the magnetic constitutive parameters were required to be spatially inhomogeneous and anisotropic, albeit at the cost of some scatterings from the hidden object. Inspired by such achievement, more cylindrical cloak works have been done, such as the scattering of the simplified cylindrical cloak [10], the hiding effect with different coordinate transformations [11], and the dispersive properties of the cylindrical cloak [12], [13].

The cylindrical cloak has been modeled by using both analytical and numerical methods. The analytical methods include wave scattering theory [14], Fourier-based approach [15], and wave expansion method [16]. The COMSOL Multiphysics is a powerful tool for the numerical simulation of the cylindrical cloak [3], which is based on the finite-element method (FEM). In contrast to FEM, finite-difference time-domain (FDTD) method [17]–[19] is based on time-domain analysis, which is more capable of dealing with electromagnetic issues containing dispersive, inhomogeneous, and anisotropic medium. As the FDTD algorithm is directly derived from Maxwell's equations, it is more accurate than other numerical methods and has been successfully applied to the modeling of cylindrical cloak as well as other types of cloaks [20], [21].

Most of the properties of the cylindrical cloak have been studied based on 2-D transformations, which means that the object can be perfectly hidden only if the incident wave is in the 2-D plane. However, a more important problem of the off-plane incident wave remains untouched. As the cloaks with 3-D constitutive parameters are unable to be demonstrated in experiments until now, it is urgent to explore the 2-D cloaks with off-plane incident wave on 3-D applications.

In this study, for the first time, a modeling theory of the 3-D cylindrical cloak based on 2-D FDTD method is derived. We have shown that it is less time consuming and memory saving (than the 3-D FDTD method), and easier to be implemented using a personal computer. Using this method, we have investigated the invisibility performance of the cloak with 2-D constitutive parameters when the incident wave is off the 2-D plane. The bistatic radar cross sections (RCS) as well as the scattered fields have been calculated to evaluate the scatterings of the object under the cloak. We have investigated the invisibility performance with different incident-wave configurations, structures, and wavelengths. We have also compared the numerical results together with their physical explanations, and the present results point out a possible way to evaluate the 2-D cloak on 3-D applications.

Fig. 1. Geometry of the cylindrical cloak, where the incident wave vector $\mathbf{k}$ is in the xz plane with its vertical plane illustrated by the yellow region, while θ is the angle between k-direction and $+x$-direction, α is the angle between $k \times y$-direction and the magnetic polarization direction, and ϕ is the azimuthal angle in the xy plane for RCS calculations. The symbols R_1 and R_2 represent the inner and outer radius of the cloak, respectively.

II. MODELING

Fig. 1 shows the geometry of our cylindrical cloak with R_1 and R_2 as inner and outer radius, respectively. The vector $\mathbf{k}$ denotes the wave vector of the incident wave, and the direction and polarization are defined by θ and α, respectively. As the cloak is axisymmetric, we set the incident wave vector in the xz plane for convenience, without loss of generality. Therefore, we know from Fig. 1 that θ is the angle between k-direction and $+x$-direction, while α is the angle between $k \times y$-direction and the magnetic polarization direction, and the yellow region represents the plane vertical with respect to the vector $\mathbf{k}$. The angle ϕ is the azimuthal angle in the xy plane, which will be useful for the RCS calculations. Based on the aforementioned definition, the TM wave and TE wave in the xy plane are modeled by $\theta = 0°, \alpha = 0°$, and $\theta = 0°, \alpha = 90°$, respectively. For the modeling of metamaterials, the FDTD grid size should be less than $1/80$ of the wavelength to keep the simulation stable and converge [21]. In the 3-D cylindrical cloak modeling, the required system resources are beyond the capability of any single personal computer [22]. In our opinion, the 3-D modeling is not necessary due to the invariance of the cylindrical cloak's parameters in the z-direction and the 2-D modeling can be used as an alternative method to save memory and time due to the components' unit length in the z-direction. Let $\mathbf{E}_i = \mathbf{E}_0 e^{j(\omega t - \mathbf{k} \cdot \mathbf{r})}$, where $\mathbf{k} = k_0 \cos\theta \hat{\mathbf{x}} + k_0 \sin\theta \hat{\mathbf{z}}$ and $k_0 = \omega\sqrt{\mu_0 \varepsilon_0}$. According to the theory that the tangential wave vectors are continuous at the interface of different media, the scattering electric component can be written as $\mathbf{E}_S = \mathbf{E}_{SA}(x, y) \exp(j\omega t - jk_0 z \sin\theta)$, and hence, $\partial/\partial z = -jk_0 \sin\theta = -j\omega\sqrt{\mu_0 \varepsilon_0}\sin\theta = -\sqrt{\mu_0 \varepsilon_0}\sin\theta \cdot \partial/\partial t$. This is the key to reduce the 3-D modeling to 2-D modeling, and we have derived our 2-D FDTD formula in the following section.

In this paper, we have studied the cloak generated by a linear coordinate transformation, and the full set of electromagnetic

parameters are [4] $\varepsilon_r = \mu_r = (r - R_1)/(r), \varepsilon_\phi = \mu_\phi = (r)/(r - R_1), \varepsilon_z = \mu_z = ((R_2)/(R_2 - R_1))^2(r - R_1)/(r)$, which we have termed as the 3-D constitutive parameters. In the 2-D case, objects can be hidden under the TM wave or TE wave as long as an ideal cloak is provided with 2-D TM constitutive parameters ($\varepsilon_r = (r - R_1)/(r), \varepsilon_\phi = (r)/(r - R_1), \mu_z = ((R_2)/(R_2 - R_1))^2(r - R_1)/(r), \mu_r = \mu_\phi = \varepsilon_z = 1$) or 2-D TE constitutive parameters ($\mu_r = (r - R_1)/(r), \mu_\phi = (r)/(r - R_1), \varepsilon_z = ((R_2)/(R_2 - R_1))^2(r - R_1)/(r), \varepsilon_r = \varepsilon_\phi = \mu_z = 1$), respectively. Even the simplest 2-D TM (or TE) constitutive parameters are hard to be achieved in experiment, which brings the use of the simplified TM constitutive parameters ($\varepsilon_r = ((R_2)/(R_2 - R_1))^2((r - R_1)/(r))^2, \varepsilon_\phi = ((R_2)/(R_2 - R_1))^2, \mu_r = \mu_\phi = \mu_z = \varepsilon_z = 1$) or simplified TE constitutive parameters [4], or even the simplified constitutive parameters based on quadratic transformations to reduce the scatterings [23], [24]. In experiment, these parameters may be realized by metamaterials [4] or photonic crystals [25], which are beyond the scope of this study.

The FDTD method starts from the two-curl Maxwell's equations, which are

$$\begin{cases} \nabla \times \mathbf{E} = -\dfrac{\partial \mathbf{B}}{\partial t} \\ \nabla \times \mathbf{H} = \dfrac{\partial \mathbf{D}}{\partial t} \end{cases} \tag{1}$$

as well as the constitutive relations $\mathbf{D} = \varepsilon \cdot \mathbf{E}, \mathbf{B} = \mu \cdot \mathbf{H}$, where $\mathbf{E}, \mathbf{H}, \mathbf{D}$, and $\mathbf{B}$ are the electric field, magnetic field, electric flux density, and magnetic flux density, respectively. From the coordinate transformations, we know that ε and μ are the second-order tensors that can be expressed as, taking ε for instance, $\varepsilon_{xx} = \varepsilon_r \cos^2\phi + \varepsilon_\phi \sin^2\phi, \varepsilon_{xy} = \varepsilon_{yx} = (\varepsilon_r - \varepsilon_\phi)\sin\phi\cos\phi, \varepsilon_{yy} = \varepsilon_r \sin^2\phi + \varepsilon_\phi \cos^2\phi$, and $\varepsilon_{zz} = \varepsilon_z$ with other components being zero, where $\varepsilon_r, \varepsilon_\phi$, and ε_z have been defined earlier and ϕ is the azimuthal angle. Notice from the 3-D constitutive parameters defined earlier that ε_r and μ_r are always less than unity so that a dispersion model (e.g., Drude model) should be applied, which can be given as, taking ε_r for instance [20]

$$\varepsilon_r(\omega) = 1 - \frac{\omega_{pr}^2}{\omega^2 - j\omega\gamma} \tag{2}$$

where ω_{pr} and γ are plasma and collision frequencies of the material for ε_r, and we use ω_{mr}, ω_{pz}, and ω_{mz} as the plasma frequencies for μ_r, ε_z, and μ_z, respectively. As ε_ϕ and μ_ϕ are always greater than unity, the dispersion model is not needed. Also, the modeling of ε_z and μ_z depends on their values. The principle is the same when modeling with the 2-D TM (TE) constitutive parameters, i.e., the Drude model is needed as long as the component of ε or μ is less than unity.

After substituting $\partial/\partial z = -\sqrt{\mu_0 \varepsilon_0}\sin\theta \cdot \partial/\partial t$ in (1), together with some auxiliary components, as

$$\begin{cases} D_{xa} = D_x - \varepsilon_0 \sin\theta H_y \\ D_{ya} = D_y + \varepsilon_0 \sin\theta H_x \\ B_{xa} = B_x + \mu_0 \sin\theta E_y \\ B_{ya} = B_y - \mu_0 \sin\theta E_x \end{cases} \tag{3}$$

we have

$$\begin{cases} \dfrac{\partial D_{xa}}{\partial t} = \sqrt{\dfrac{\varepsilon_0}{\mu_0}} \dfrac{\partial H_z}{\partial y} \\[6pt] \dfrac{\partial D_{ya}}{\partial t} = \sqrt{\dfrac{\varepsilon_0}{\mu_0}} \dfrac{\partial H_z}{\partial x} \\[6pt] \dfrac{\partial D_z}{\partial t} = \sqrt{\dfrac{\varepsilon_0}{\mu_0}} \left(\dfrac{\partial H_y}{\partial x} - \dfrac{\partial H_x}{\partial y} \right) \\[6pt] \dfrac{\partial B_{xa}}{\partial t} = \sqrt{\dfrac{\mu_0}{\varepsilon_0}} \dfrac{\partial E_z}{\partial y} \\[6pt] \dfrac{\partial B_{ya}}{\partial t} = \sqrt{\dfrac{\mu_0}{\varepsilon_0}} \dfrac{\partial E_z}{\partial x} \\[6pt] \dfrac{\partial B_z}{\partial t} = \sqrt{\dfrac{\mu_0}{\varepsilon_0}} \left(\dfrac{\partial E_x}{\partial y} - \dfrac{\partial E_y}{\partial x} \right). \end{cases} \tag{4}$$

Notice that in the derivation of (4), we have used the normalization [18] of $\mathbf{E}' = \mathbf{E}\sqrt{\varepsilon_0/\mu_0}$ and $\mathbf{D}' = \mathbf{D}\sqrt{\varepsilon_0/\mu_0}$ to alter the electric and magnetic field into the same order of magnitude in order to make the FDTD simulation more accurate, and then replaced $\mathbf{E}'$ and $\mathbf{D}'$ with $\mathbf{E}$ and $\mathbf{D}$ in writing (4). It is easy to discretize (4) to get the FDTD updating equations; however, we have not listed them here to save space.

Subsequently, we have substituted the expressions of ε and μ together with the constitutive relations $\mathbf{D} = \varepsilon \cdot \mathbf{E}$ and $\mathbf{B} = \mu \cdot \mathbf{H}$ into (3) to obtain the key equations for the cloak modeling after some derivations, as follows:

$$\left[\begin{pmatrix} \mu_{xy} & -\mu_{xx} \\ \mu_{yy} & -\mu_{yx} \end{pmatrix} \begin{pmatrix} \varepsilon_{xx} & \varepsilon_{xy} \\ \varepsilon_{yx} & \varepsilon_{yy} \end{pmatrix} \right.$$
$$\left. + \begin{pmatrix} 0 & \sin^2\theta \\ -\sin^2\theta & 0 \end{pmatrix} \right] \begin{pmatrix} E_x \\ E_y \end{pmatrix}$$
$$= \frac{\sin\theta}{\mu_0} \begin{pmatrix} B_{xa} \\ B_{ya} \end{pmatrix} + \frac{1}{\varepsilon_0} \begin{pmatrix} \mu_{xy} & -\mu_{xx} \\ \mu_{yy} & -\mu_{yx} \end{pmatrix} \begin{pmatrix} D_{xa} \\ D_{ya} \end{pmatrix} \tag{5a}$$

$$\left[\begin{pmatrix} \varepsilon_{xy} & -\varepsilon_{xx} \\ \varepsilon_{yy} & -\varepsilon_{yx} \end{pmatrix} \begin{pmatrix} \mu_{xx} & \mu_{xy} \\ \mu_{yx} & \mu_{yy} \end{pmatrix} \right.$$
$$\left. + \begin{pmatrix} 0 & \sin^2\theta \\ -\sin^2\theta & 0 \end{pmatrix} \right] \begin{pmatrix} H_x \\ H_y \end{pmatrix}$$
$$= -\frac{\sin\theta}{\varepsilon_0} \begin{pmatrix} D_{xa} \\ D_{ya} \end{pmatrix} + \frac{1}{\mu_0} \begin{pmatrix} \varepsilon_{xy} & -\varepsilon_{xx} \\ \varepsilon_{yy} & -\varepsilon_{yx} \end{pmatrix} \begin{pmatrix} B_{xa} \\ B_{ya} \end{pmatrix}. \tag{5b}$$

To solve (5a) and (5b), we have separated them into two groups. Let us first consider (5a). With regard to the expressions of ε_{xx}, etc., as well as by applying the auxiliary differential equation method [18] $(j\omega \rightarrow \partial/\partial t)$, (5a) can be simplified as shown in (6a) at the bottom of the page, where the coefficients are defined in Table I as follows:

$$f(\eta, \theta, \phi, \varepsilon_\phi, \mu_\phi, p, q, m)$$
$$= \eta \left[\frac{(2 + m\gamma\Delta t)(\varepsilon_\phi \sin^2\phi + \mu_\phi \cos^2\phi - \sin^2\theta)}{2\Delta t^2} \right.$$
$$\left. + \frac{(\varepsilon_\phi p\omega_{mr}^2 \sin^2\phi + \mu_\phi q\omega_{pr}^2 \cos^2\phi)}{4} \right]$$

$$g(\eta, \phi, \varepsilon_\phi, \mu_\phi, p, q, m)$$
$$= \eta \sin\phi \cos\phi \left[\frac{(2 + m\gamma\Delta t)(\varepsilon_\phi - \mu_\phi)}{2\Delta t^2} \right.$$
$$\left. + \frac{(\varepsilon_\phi p\omega_{mr}^2 - \mu_\phi q\omega_{pr}^2)}{4} \right]$$

$$F_1 = \frac{(2 + \gamma\Delta t)\sin\theta}{2\mu_0\Delta t^2} \quad F_2 = \frac{2\sin\theta}{\mu_0\Delta t^2}$$
$$F_3 = \frac{(2 - \gamma\Delta t)\sin\theta}{2\mu_0\Delta t^2}.$$

The modeling procedure of H_x and H_y is the same as that of E_x and E_y, which can be derived from (5b), and the updating equations are given as shown in (6b) at the bottom of the page, where the coefficients are defined in Table II as follows:

$$P_1 = -\frac{(2 + \gamma\Delta t)\sin\theta}{2\varepsilon_0\Delta t^2} \quad P_2 = -\frac{2\sin\theta}{\varepsilon_0\Delta t^2}$$
$$P_3 = -\frac{(2 - \gamma\Delta t)\sin\theta}{2\varepsilon_0\Delta t^2}.$$

Now, let us discuss the modeling of E_z and H_z from $D_z = \varepsilon_0\varepsilon_z E_z$ and $B_z = \mu_0\mu_z H_z$, where ε_z and μ_z can be either greater or less than unity, depending on the location in the cloak. The modeling procedure of H_z is the same as that of E_z. In the case of $\varepsilon_z \geq 1$, E_z is directly obtained by $E_z = (D_z)/(\varepsilon_0\varepsilon_z)$. For $\varepsilon_z < 1$, the Drude model is applied as that of (2), and

$$\begin{pmatrix} E_x^{n+1} \\ E_y^{n+1} \end{pmatrix} = \begin{pmatrix} A_1 & -C_1 \\ C_1 & J_1 \end{pmatrix}^{-1}$$
$$\cdot \left[\begin{pmatrix} A_2 & -C_2 \\ C_2 & J_2 \end{pmatrix} \begin{pmatrix} E_x^n \\ E_y^n \end{pmatrix} - \begin{pmatrix} A_3 & -C_3 \\ C_3 & J_3 \end{pmatrix} \begin{pmatrix} E_x^{n-1} \\ E_y^{n-1} \end{pmatrix} + \begin{pmatrix} G_1 & -I_1 \\ I_1 & -K_1 \end{pmatrix} \begin{pmatrix} D_{xa}^{n+1} \\ D_{ya}^{n+1} \end{pmatrix} - \right.$$
$$\left. \begin{pmatrix} G_2 & -I_2 \\ I_2 & -K_2 \end{pmatrix} \begin{pmatrix} D_{xa}^n \\ D_{ya}^n \end{pmatrix} + \begin{pmatrix} G_3 & -I_3 \\ I_3 & -K_3 \end{pmatrix} \begin{pmatrix} D_{xa}^{n-1} \\ D_{ya}^{n-1} \end{pmatrix} + \begin{pmatrix} F_1 B_{ya}^{n+1} - F_2 B_{ya}^n + F_3 B_{ya}^{n-1} \\ F_1 B_{xa}^{n+1} - F_2 B_{xa}^n + F_3 B_{xa}^{n-1} \end{pmatrix} \right] \tag{6a}$$

$$\begin{pmatrix} H_x^{n+1} \\ H_y^{n+1} \end{pmatrix} = \begin{pmatrix} M_1 & -N_1 \\ N_1 & S_1 \end{pmatrix}^{-1}$$
$$\cdot \left[\begin{pmatrix} M_2 & -N_2 \\ N_2 & S_2 \end{pmatrix} \begin{pmatrix} H_x^n \\ H_y^n \end{pmatrix} - \begin{pmatrix} M_3 & -N_3 \\ N_3 & S_3 \end{pmatrix} \begin{pmatrix} H_x^{n-1} \\ H_y^{n-1} \end{pmatrix} + \begin{pmatrix} Q_1 & -R_1 \\ R_1 & -T_1 \end{pmatrix} \begin{pmatrix} B_{xa}^{n+1} \\ B_{ya}^{n+1} \end{pmatrix} - \right.$$
$$\left. \begin{pmatrix} Q_2 & -R_2 \\ R_2 & -T_2 \end{pmatrix} \begin{pmatrix} B_{xa}^n \\ B_{ya}^n \end{pmatrix} + \begin{pmatrix} Q_3 & -R_3 \\ R_3 & -T_3 \end{pmatrix} \begin{pmatrix} B_{xa}^{n-1} \\ B_{ya}^{n-1} \end{pmatrix} + \begin{pmatrix} P_1 D_{ya}^{n+1} - P_2 D_{ya}^n + P_3 D_{ya}^{n-1} \\ P_1 D_{xa}^{n+1} - P_2 D_{xa}^n + P_3 D_{xa}^{n-1} \end{pmatrix} \right] \tag{6b}$$

TABLE I
COEFFICIENTS DEFINED IN (6A)

ξ	f/g	η	θ	ϕ	ε_ϕ	μ_ϕ	p	q	m
A_1	f	1	θ	ϕ	ε_ϕ	μ_ϕ	1	1	1
A_2	f	2	θ	ϕ	ε_ϕ	μ_ϕ	-1	-1	0
A_3	f	1	θ	ϕ	ε_ϕ	μ_ϕ	1	1	-1
C_1	g	1	-	ϕ	ε_ϕ	μ_ϕ	1	1	1
C_2	g	2	-	ϕ	ε_ϕ	μ_ϕ	-1	-1	0
C_3	g	1	-	ϕ	ε_ϕ	μ_ϕ	1	1	-1
G_1	f	$1/\varepsilon_0$	0	ϕ	1	μ_ϕ	1	0	1
G_2	f	$2/\varepsilon_0$	0	ϕ	1	μ_ϕ	-1	0	0
G_3	f	$1/\varepsilon_0$	0	ϕ	1	μ_ϕ	1	0	-1
I_1	g	$1/\varepsilon_0$	-	ϕ	1	μ_ϕ	1	0	1
I_2	g	$2/\varepsilon_0$	-	ϕ	1	μ_ϕ	-1	0	0
I_3	g	$1/\varepsilon_0$	-	ϕ	1	μ_ϕ	1	0	-1
J_1	f	-1	θ	$\phi+\pi/2$	ε_ϕ	μ_ϕ	1	1	1
J_2	f	-2	θ	$\phi+\pi/2$	ε_ϕ	μ_ϕ	-1	-1	0
J_3	f	-1	θ	$\phi+\pi/2$	ε_ϕ	μ_ϕ	1	1	-1
K_1	f	$1/\varepsilon_0$	0	$\phi+\pi/2$	1	μ_ϕ	1	0	1
K_2	f	$2/\varepsilon_0$	0	$\phi+\pi/2$	1	μ_ϕ	-1	0	0
K_3	f	$1/\varepsilon_0$	0	$\phi+\pi/2$	1	μ_ϕ	1	0	-1

TABLE II
COEFFICIENTS DEFINED IN (6B)

ξ	f/g	η	θ	ϕ	ε_ϕ	μ_ϕ	p	q	m
M_1	f	1	θ	$\phi+\pi/2$	ε_ϕ	μ_ϕ	1	1	1
M_2	f	2	θ	$\phi+\pi/2$	ε_ϕ	μ_ϕ	-1	-1	0
M_3	f	1	θ	$\phi+\pi/2$	ε_ϕ	μ_ϕ	1	1	-1
N_1	g	-1	-	ϕ	ε_ϕ	μ_ϕ	1	1	1
N_2	g	-2	-	ϕ	ε_ϕ	μ_ϕ	-1	-1	0
N_3	g	-1	-	ϕ	ε_ϕ	μ_ϕ	1	1	-1
Q_1	f	$1/\mu_0$	0	$\phi+\pi/2$	ε_ϕ	1	0	1	1
Q_2	f	$2/\mu_0$	0	$\phi+\pi/2$	ε_ϕ	1	0	-1	0
Q_3	f	$1/\mu_0$	0	$\phi+\pi/2$	ε_ϕ	1	0	1	-1
R_1	g	$-1/\mu_0$	-	ϕ	ε_ϕ	1	0	1	1
R_2	g	$-2/\mu_0$	-	ϕ	ε_ϕ	1	0	-1	0
R_3	g	$-1/\mu_0$	-	ϕ	ε_ϕ	1	0	1	-1
S_1	f	-1	θ	ϕ	ε_ϕ	μ_ϕ	1	1	1
S_2	f	-2	θ	ϕ	ε_ϕ	μ_ϕ	-1	-1	0
S_3	f	-1	θ	ϕ	ε_ϕ	μ_ϕ	1	1	-1
T_1	f	$1/\mu_0$	0	ϕ	ε_ϕ	1	0	1	1
T_2	f	$2/\mu_0$	0	ϕ	ε_ϕ	1	0	-1	0
T_3	f	$1/\mu_0$	0	ϕ	ε_ϕ	1	0	1	-1

we have (7), shown at the bottom of the page. Here, the superscripts n and Δt represent the discrete time step. Therefore, the cloak can be modeled by two steps: first, by updating the auxiliary components as (4), and then by updating the electric and magnetic components as (6a)–(6b) and (7). If we set $\theta = \alpha = 0°$ which means the in-plane incidence, our FDTD updating equations are consistent with the 2-D FDTD equations obtained in [21].

III. RESULTS AND DISCUSSIONS

In this section, we apply the theory developed in the previous section to our FDTD calculations by home-generated codes [26] and study the invisibility performance of the cloak with different incident configurations and structures. To evaluate the cloaking performance, the scattering effect of the hidden objects needs to be calculated, which is usually represented by the bistatic RCS defined as follows [18]:

$$\mathrm{RCS}(\phi) = 10\lg\left(\frac{2\pi r}{\lambda}\frac{|E_s(\phi)|^2}{|E_\mathrm{inc}|^2}\right) \text{ (dB)} \qquad (8)$$

where $|E_s(\phi)|^2$ is the power scattered per unit angle in direction ϕ (ranging from $0°$ to $360°$) and $|E_\mathrm{inc}|^2$ is the incident power per unit length. By using the total field/scattered field (TF/SF) method [18], the information of the scattered field can be extracted, which is the basis for the near-to-far-field transformation. Then, the information of the far-field as well as the RCS results can be obtained.

In the following simulations, we have chosen an incident plane wave with amplitude of unity propagating from $-x$- to $+x$-direction (in the 2-D projected coordinate), which can be easily realized by the TF/SF method. The interior surface of the cloak is coated with perfect electromagnetic conductor (PEMC) to exclude both TE and TM incident waves, as we need to deal with incident waves of any angle and polarization. It is in contrast with the choice made in the other works [10]–[13], [20], [21], where the region of $r < R_1$ is filled with perfect electric conductor because they only deal with an incident TM wave. The cell size was chosen as $\Delta x = \Delta y = \lambda/100$ for the case of $R_1 = 0.02$ m and 0.05 m, while $\lambda/250$ for the case of $R_1 = 0.08$ m since a thinner cloak. In all the calculations, $\Delta t = 0.5\Delta x/c$, where c is the speed of light in free space, and 20 000 time steps calculations were performed. Since we did not focus on the losses in this study, γ was set to be 0 for simplicity.

A. Invisibility Performance on the Incident Polarization

We first investigated the invisibility performance with different incident polarizations. The incident angle θ was fixed at $0°$, which means the incident wave is in the xy plane. We chose the 2-D TM constitutive parameters with structure parameters as follows: $R_1 = 0.05$ m, $R_2 = 0.1$ m, and $\mathrm{wavelength} = 0.1$ m. We tested the invisibility performance on the incident polarizations by changing α.

$$\begin{cases} E_z^{n+1} = \left(\frac{8-2\omega_{pz}^2\Delta t^2}{4+2\gamma\Delta t+\omega_{pz}^2\Delta t^2}\right)E_z^n - \left(\frac{4-2\gamma\Delta t+\omega_{pz}^2\Delta t^2}{4+2\gamma\Delta t+\omega_{pz}^2\Delta t^2}\right)E_z^{n-1} \\ \qquad + \frac{1}{\varepsilon_0\left(4+2\gamma\Delta t+\omega_{pz}^2\Delta t^2\right)}\left[(4+2\gamma\Delta t)D_z^{n+1} - 8D_z^n + (4-2\gamma\Delta t)D_z^{n-1}\right] \\ H_z^{n+1} = \left(\frac{8-2\omega_{mz}^2\Delta t^2}{4+2\gamma\Delta t+\omega_{mz}^2\Delta t^2}\right)H_z^n - \left(\frac{4-2\gamma\Delta t+\omega_{mz}^2\Delta t^2}{4+2\gamma\Delta t+\omega_{mz}^2\Delta t^2}\right)H_z^{n-1} \\ \qquad + \frac{1}{\mu_0(4+2\gamma\Delta t+\omega_{mz}^2\Delta t^2)}\left[(4+2\gamma\Delta t)B_z^{n+1} - 8B_z^n + (4-2\gamma\Delta t)B_z^{n-1}\right]. \end{cases} \qquad (7)$$
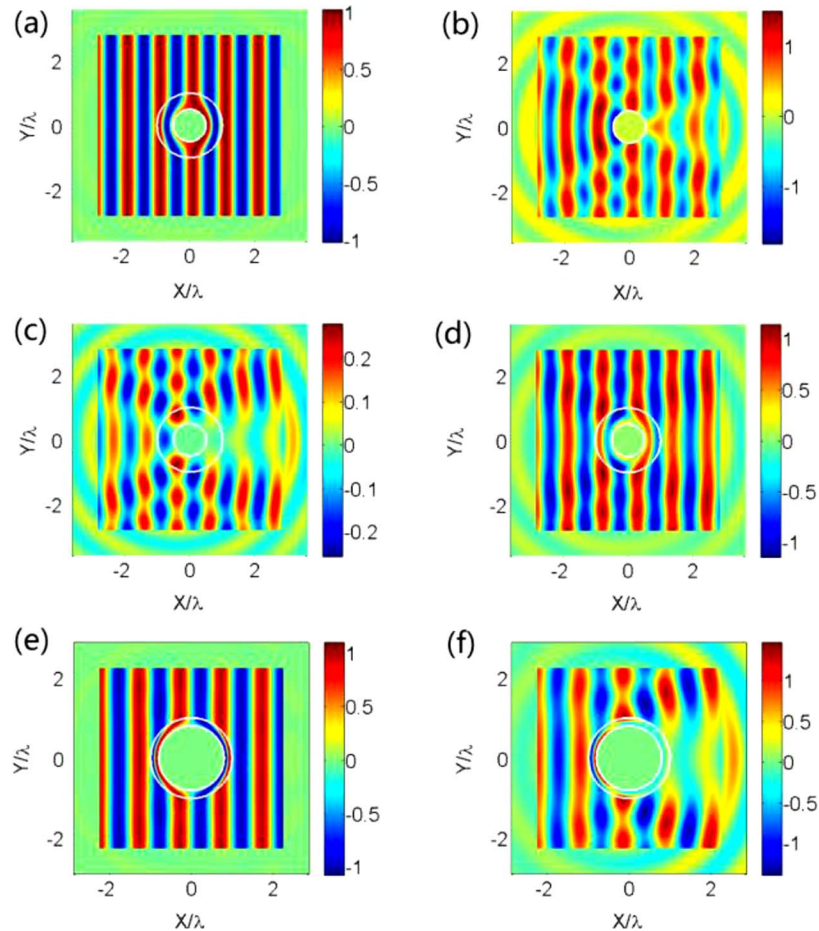
Fig. 2.   (a) H_z field with $R_1 = 0.05$ m, $R_2 = 0.1$ m, $\alpha = 0°, \theta = 0°$. (b) Same as that of (a), but the cloak is removed. (c) E_z field with $R_1 = 0.05$ m, $R_2 = 0.1$ m, $\alpha = 10°, \theta = 0°$. (d) Same as that of (a), but $\theta = 20°$. (e) and (f) H_z fields with $R_1 = 0.08$ m, $R_2 = 0.1$ m, $\alpha = 0°, \theta = 0°$ and $20°$, respectively. In all the cases, the incident wavelength is fixed at 0.1 m with amplitude of unity and 2-D TM constitutive parameters are chosen. Notice that the TF/SF method is used so that the scattered fields can be seen directly outside the rectangular frame.

It is obvious that the TM wave ($\alpha = 0°$) is bent and guided around the cloak region perfectly, which can be seen in Fig. 2(a) as the field of H_z component, where the two white circles represent the inner and outer radius of the cloak. Note that the TF/SF method is used and the scattered fields can be seen directly as the fields outside the rectangular frame in Fig. 2. The corresponding RCS is given by the black curve in Fig. 3(a), where the residual RCS is attributed to the numerical error from the discretization of Maxwell's equations, since the RCS should be infinitely small owing to the lack of scatterings from the ideal cloak. We also calculated the case of the real scatterings in which the structures were the same as those presented in Fig. 2(a), except the removal of the cloak, and the field pattern is presented in Fig. 2(b), with its RCS results illustrated by the red-dashed curve in Fig. 3(b). By comparing the black curve and red-dashed curve, it can be noted that an RCS reduction of about 20 dB (even more for some other directions) is achieved by the ideal cloak. The numerical errors are relatively small that will not affect the validity of our calculations.

Considering the invisibility performance of the cloak as a function of α, we found that the invisibility performance becomes worse with increasing α. The corresponding RCS results are given in Fig. 3(a) by the red ($\alpha = 10°$), blue ($\alpha = 20°$), and green ($\alpha = 30°$) curves. In the case of $\alpha = 10°$, as shown

in Fig. 2(c), in the E_z field, no cloaking effect is found. However, in the same case, the H_z field is identical to that shown in Fig. 2(a) and can be explained as follows. With the 2-D TM constitutive parameters, objects can be perfectly hidden under TM incident wave ($\alpha = 0°$), because impedance matching occurs everywhere in the xy plane. However, for the TE incident wave ($\alpha = 90°$), there is no cloaking effect, where, in other words, the cloak just means air and there is large scatterings from the PEMC because of the impedance mismatch at the surface of the PEMC. An incident wave in the xy plane can be decomposed into TE and TM waves, and the greater the value of α, the stronger the TE component wave, and hence, the invisibility performance gets worse with the increase in α.

To summarize the RCS results in this section, we plotted the forward RCS ($\phi = 0°$) as a function of α, as shown in Fig. 4(a), which were chosen as a criterion of the invisibility performance. The invisibility performance became worse with the increase in α.

B. Invisibility Performance on the Incident Angle and Structure

In this section, we have investigated the invisibility performance of the cloak as a function of the incident angle. We chose
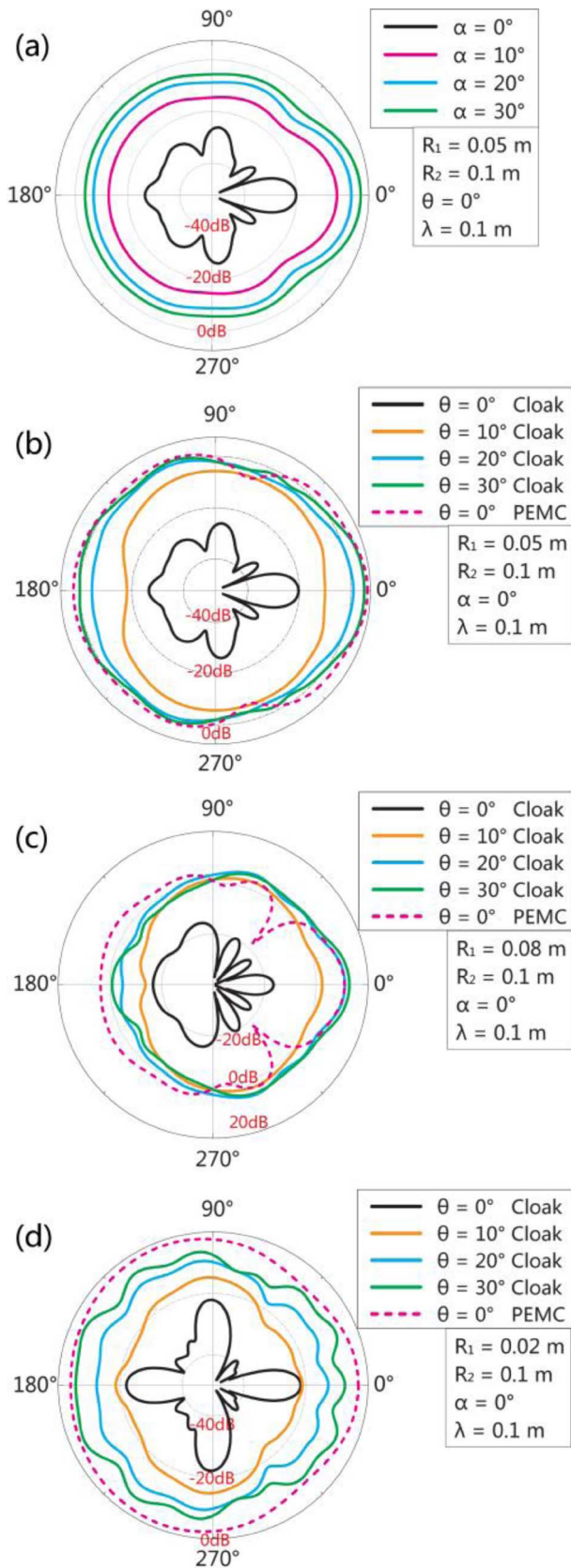
Fig. 3. RCS results under different incident configurations and structures, which are (a) $R_1 = 0.05$ m, $R_2 = 0.1$ m, and $\theta = 0°$. (b) $R_1 = 0.05$ m, $R_2 = 0.1$ m, and $\alpha = 0°$. (c) $R_1 = 0.08$ m, $R_2 = 0.1$ m, and $\alpha = 0°$. (d) $R_1 = 0.02$ m, $R_2 = 0.1$ m, and $\alpha = 0°$. In all the cases, the wavelength is fixed at 0.1 m and 2-D TM constitutive parameters are chosen.
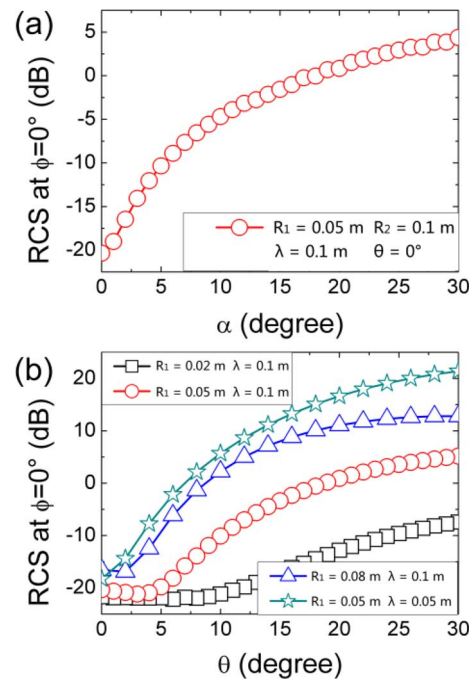
Fig. 4. Forward RCS results ($\phi = 0°$) with different incident configurations and structures, which are (a) $R_1 = 0.05$ m, $R_2 = 0.1$ m, $\theta = 0°$, and wavelength $= 0.1$ m. (b) $R_2 = 0.1$ m and $\alpha = 0°$, while R_1 and the wavelength are indicated in the figure. In all the cases, the 2-D TM constitutive parameters are chosen.

three different cloak structures and fixed α at $0°$ for the optimized invisibility performance based on our previous discussion. Structure 1 has $R_1 = 0.05$ m, $R_2 = 0.1$ m, wavelength $= 0.1$ m, and the 2-D TM constitutive parameters similar to those presented in the previous section. Fig. 2(a) also shows the H_z field for the case of $\theta = 0°$. We tested the invisibility performance by changing θ, where the incident wave was off the plane and the cloaking effect was not perfect. In Fig. 3(b), the RCS of $\theta = 10°, 20°$, and $30°$ are illustrated by yellow, blue, and green curves, respectively. The invisibility performance became worse with the increase in θ.

The physical essence can be understood from Fig. 1. As the incident wave vector is in the xz plane and $\alpha = 0°$, the incident wave can be regarded as a TM wave in the ky plane. It can be decomposed as two waves propagating in the $+x$- and $+z$-directions, respectively, or more generally, two TM waves named TM_1 and TM_2 in the xy and yz planes, respectively. From the discussion presented in the previous section, it can be noted that objects are perfectly hidden under TM_1 wave, whereas no cloaking effect occurs under TM_2 wave. The latter conclusion comes from the fact that the TM_2 wave in the yz plane considers the cloak and PEMC as scatterers because we have $\mu_{xx} = \varepsilon_{zz} = 1$ under our 2-D TM constitutive parameters. However, we must clarify that unlike the TE wave mentioned earlier, here, we have $\varepsilon_{yy} \neq 1$ in the cloak region, and hence, we cannot regard the cloak as air under the TM_2 wave, but only as some scatterers, which means, in other words, that the structure is not just a PEMC for the TM_2 wave. However, the TM_2 wave is still the only reason for the deterioration of the invisibility performance with the increase in θ.

Then, we investigated the case of Structure 2 with inner radius of the cloak $R_1 = 0.08$ m and other parameters remaining the same, corresponding to a thinner cloak. In this case, the H_z fields with $\theta = 0°$ and $\theta = 20°$ are given in Fig. 2(e) and (f), and the corresponding RCS results are given in Fig. 3(c). On comparing Fig. 2(f) with (d), or Fig. 3(c) with Fig. 3(b), one can conclude that a better invisibility performance is obtained with a thicker cloak for the same incident wave (angle and polarization) and outer cloak radius. This can be explained as follows. We had clarified that when $\theta > 0°$, there are scatterings caused by the TM_2 wave; hence, under the same outer radius R_2 and wavelength, larger PEMC (=thinner cloak) may cause larger scatterings, together with worse invisibility performance. The aforementioned explanations can be further supported by testing a thicker cloak with better invisibility performance named Structure 3 with $R_1 = 0.02$ m and other parameters remaining the same, with the corresponding RCS results given in Fig. 3(d). To summarize, we plotted the forward RCS ($\phi = 0°$) as a function of the incident angle θ, as shown in Fig. 4(b).

Here, for the first time, we have introduced the concept of invisibility angle to evaluate the cloaking performance. The forward RCS ($\phi = 0°$) with incident wave on the xy plane ($\theta = 0°$) has been taken as a criterion and we have defined an incident angle θ_0 as the invisibility angle, if the forward RCS is 10 dB higher than the criterion. From the RCS definition in (8), it can be noted that the RCS depends on the intensity of the scattered field, which indicates that under our defined invisibility angle θ_0, the intensity of the forward scattered field is one order greater than that of the criterial case ($\theta = 0°$). By applying the definition to Fig. 4, one can find that the invisibility angle of the three cases ($R_1 = 0.02, 0.05,$ and 0.08 m) are about $22°$, $10°$, and $6°$, respectively, which again supports our conclusion that thicker cloak has larger invisibility angle. With the same principle, it can be found from Fig. 4(a) that the invisibility polarization angle α_0 (at which the forward RCS is 10 dB higher than that with $\alpha = 0°$ when θ is fixed at $0°$) of the structure is about $5°$.

At the end of this section, we have presented a discussion on the polarization angle α. In the case of both α and θ greater than $0°$, the incident wave can be decomposed as a TE and a TM wave in the ky plane. Moreover, the two waves can be decomposed as TE_1 and TM_1 wave in the xy plane as well as TE_2 and TM_2 wave in the yz plane. Thus, the scatterings in this case are from the TE_1, TE_2, and TM_2 waves, where the invisibility performance may be even worse.

C. Invisibility Performance on the Wavelength

We now varied the wavelength from 0.1 to 0.05 m with other parameters remaining the same for Structure 1, where $R_1 = 0.05$ m and $R_2 = 0.1$ m. The corresponding forward RCS results toward incident angle θ are given by the green curve in Fig. 4(b). When compared with the red curve, it can be observed that as the wavelength decreases from 0.1 to 0.05 m, the invisibility angle dramatically drops from $10°$ to $4°$. This is because the same PEMC causes larger scatterings under the TM_2 wave with smaller wavelength.

At the end of Section III, we give a comparison of our FDTD results with those obtained by other literatures to validate our proposed formula and results. On one side, the field patterns by our FDTD code [e.g., Fig. 2(a), (c), and (e)] are consistent with the results obtained by other FDTD codes [12], [21], FEM method [23], and analytical method [16]. On the other side, our RCS result without cloak [red-dashed line in Fig. 3(c)] is nearly the same as that in [10], and although with different calculation parameters, our RCS results with cloak are comparable with those obtained by another literature [10], [11], [20], since both RCS possess many maximums and minimums.

IV. CONCLUSION

In summary, we have derived a theory for the modeling of the 3-D cylindrical cloak based on 2-D FDTD method, which is less time consuming, memory saving, and easy to be implemented by personal computer, when compared with the 3-D modeling. The method has been applied to investigate the invisibility performance of the cloak with 2-D constitutive parameters toward polarization, incident angle, structure, and wavelength. The bistatic RCS as well as the scattered fields have been calculated to evaluate the scatterings of the PEMC under the cloak, from which the invisibility performance has been found to get worse with the increase in the incident angle, while the defined invisibility angle has been found to diminish with the decrease in the cloak thickness and wavelength. The physical reason for these conclusions lies in the scatterings from the PEMC under the TM_2 wave. The present results point out a possible way to evaluate the 2-D cloak on 3-D applications.

REFERENCES

[1] J. B. Pendry, D. Schurig, and D. R. Smith, "Controlling electromagnetic fields," *Science*, vol. 312, no. 5781, pp. 1780–1782, Jun. 2006.

[2] U. Leonhardt and T. G. Philbin, "Transformation optics and the geometry of light," *Prog. Opt.*, vol. 53, pp. 69–152, 2009.

[3] H. Y. Chen, C. T. Chan, and P. Sheng, "Transformation optics and metamaterials," *Nature Mater.*, vol. 9, no. 5, pp. 387–396, May 2010.

[4] D. Schurig, J. J. Mock, B. J. Justice, S. A. Cummer, J. B. Pendry, A. F. Starr, and D. R. Smith, "Metamaterial electromagnetic cloak at microwave frequencies," *Science*, vol. 314, no. 5801, pp. 977–980, Nov. 2006.

[5] R. Liu, C. Ji, J. J. Mock, J. Y. Chin, T. J. Cui, and D. R. Smith, "Broadband ground-plane cloak," *Science*, vol. 323, no. 5912, pp. 366–369, Jan. 2009.

[6] T. Ergin, N. Stenger, P. Brenner, J. B. Pendry, and M. Wegener, "Three-dimensional invisibility cloak at optical wavelengths," *Science*, vol. 328, no. 5976, pp. 337–339, Apr. 2010.

[7] J. S. Li and J. B. Pendry, "Hiding under the carpet: A new strategy for cloaking," *Phys. Rev. Lett.*, vol. 101, no. 20, pp. 203901-1–203901-4, Nov. 2008.

[8] D. Schurig, J. B. Pendry, and D. R. Smith, "Calculation of material properties and ray tracing in transformation media," *Opt. Exp.*, vol. 14, no. 21, pp. 9794–9804, Oct. 2006.

[9] J. Valentine, J. S. Li, T. Zentgraf, G. Bartal, and X. Zhang, "An optical cloak made of dielectrics," *Nature Mater.*, vol. 8, no. 7, pp. 568–571, Jul. 2009.

[10] M. Yan, Z. C. Ruan, and M. Qiu, "Scattering characteristics of simplified cylindrical invisibility cloaks," *Opt. Exp.*, vol. 15, no. 26, pp. 17772–17782, Dec. 2007.

[11] J. J. Zhang, Y. Luo, and N. A. Mortensen, "Minimizing the scattering of a nonmagnetic cloak," *Appl. Phys. Lett.*, vol. 96, no. 11, pp. 113511-1–113511-3, Mar. 2010.

[12] P. J. Yao, Z. X. Liang, and X. Y. Jiang, "Limitation of the electromagnetic cloak with dispersive material," *Appl. Phys. Lett.*, vol. 92, no. 3, pp. 031111-1–031111-3, Jan. 2008.

[13] Z. X. Liang, P. J. Yao, X. W. Sun, and X. Y. Jiang, "The physical picture and the essential elements of the dynamical process for dispersive cloaking structures," *Appl. Phys. Lett.*, vol. 92, no. 13, pp. 131118-1–131118-3, Mar. 2008.

[14] B. Zhang, H. S. Chen, B. I. Wu, Y. Luo, L. X. Ran, and J. A. Kong, "Response of a cylindrical invisibility cloak to electromagnetic waves," *Phys. Rev. B*, vol. 76, no. 12, pp. 121101-1–121101-4, Sep. 2007.

[15] A. Nicolet, F. Zolla, and S. Guenneau, "Electromagnetic analysis of cylindrical cloaks of an arbitrary cross section," *Opt. Lett.*, vol. 33, no. 14, pp. 1584–1586, Jul. 2008.

[16] Z. Ruan, M. Yan, C. W. Neff, and M. Qiu, "Ideal cylindrical cloak: Perfect but sensitive to tiny perturbations," *Phys. Rev. Lett.*, vol. 99, no. 11, pp. 113903-1–113903-4, Sep. 2007.

[17] K. Hwang and J. Ihm, "A stable fourth-order FDTD method for modeling electrically long dielectric waveguides," *J. Lightw. Technol.*, vol. 24, no. 2, pp. 1048–1056, Feb. 2006.

[18] A. Taflove, *Advances in Computational Electrodynamics: The Finite-Difference Time-Domain Method*. London, U.K.: Artech House, 1998.

[19] Z. Lin, C. Zhang, P. Ou, Y. Jia, and L. Feng, "A generally optimized FDTD model for simulating arbitrary dispersion based on the Maclaurin series expansion," *J. Lightw. Technol.*, vol. 28, no. 19, pp. 2843–2850, Oct. 2010.

[20] Y. Zhao, C. Argyropoulos, and Y. Hao, "Full-wave finite-difference time-domain simulation of electromagnetic cloaking structures," *Opt. Exp.*, vol. 16, no. 9, pp. 6717–6730, Apr. 2008.

[21] C. Argyropoulos, Y. Zhao, and Y. Hao, "A radially-dependent dispersive finite-difference time-domain method for the evaluation of electromagnetic cloaks," *IEEE Trans. Antennas Propag.*, vol. 57, no. 5, pp. 1432–1441, May 2009.

[22] Y. Zhao and Y. Hao, "Full-wave parallel dispersive finite-difference time-domain modeling of three-dimensional electromagnetic cloaking structures," *J. Comput. Phys.*, vol. 228, no. 19, pp. 7300–7312, Oct. 2009.

[23] H. Y. Chen, J. Ng, C. W. J. Lee, Y. Lai, and C. T. Chan, "General transformation for the reduced invisibility cloak," *Phys. Rev. B*, vol. 80, no. 8, pp. 085112-1–085112-4, Aug. 2009.

[24] W. Cai, U. K. Chettiar, A. V. Kildishev, V. M. Shalaev, and G. W. Milton, "Nonmagnetic cloak with minimized scattering," *Appl. Phys. Lett.*, vol. 91, no. 11, pp. 111105-1–111105-3, Sep. 2007.

[25] Y. A. Urzhumov and D. R. Smith, "Transformation optics with photonic bandgap media," *Phys. Rev. Lett.*, vol. 105, no. 16, pp. 163901-1–163901-4, Oct. 2010.

[26] X. L. Zhang, J. Feng, J. F. Song, X. B. Li, and H. B. Sun, "Grating amplitude effect on electroluminescence enhancement of corrugated organic light-emitting devices," *Opt. Lett.*, vol. 36, no. 19, pp. 3915–3917, Oct. 2011.

Xu-Lin Zhang received the B.S. degree in electronic information and science technology from the College of Electronic Science and Engineering, Jilin University, Changchun, China, in 2009, where he is currently working toward the Ph.D. degree.

His current research interests are in the area of transformation optics based optoelectronics devices.

Jun-Feng Song received the B.S. and Ph.D. degrees from the College of Electronic Science and Engineering, Jilin University, Changchun, China, in 1993 and 2000, respectively.

He was a Postdoctoral Researcher in the Changchun Institute of Optics, Chinese Academy of Sciences during 2000–2002. He is currently a Professor with Jilin University. His current research interests include silicon-based optics devices, photonic crystal fibers, and wavelength shifters.

Xian-Bin Li received the B.S. and Ph.D. degrees in microelectronics from the College of Electronic Science and Engineering, Jilin University, Changchun, China, in 2005 and 2010, respectively.

He is currently a Lecturer in Jilin University. His research interests mainly focus on the key problems in microelectronics and optoelectronics with the first-principle calculation.

Hong-Bo Sun (M'99) received the B.S. and Ph.D. degrees in electronics from Jilin University, Changchun, China, in 1992 and 1996, respectively.

He was a Postdoctoral Researcher in Satellite Venture Business Laboratory, University of Tokushima, Tokushima, Japan, from 1996 to 2000. He then joined the Department of Applied Physics, Osaka University, Osaka, Japan, as an Assistant Professor. In 2005, he was promoted as a Full Professor (Changjiang Scholar) at Jilin University. His current research interests include laser nanofabrication and ultrafast spectroscopy. By laser micronanofabrication technologies, various micro-optical, microelectronical, micromechanical, microoptoelectronic, microfluidic components, and integrated systems have been produced, while the ultrafast dynamics solar cells, organic light-emitting devices, and low-dimensional quantum systems have been deeply studied. So far, he has published over 100 scientific papers in the above field, which have been cited for more than 3500 times according to ISI search report.

Dr. Sun became a Project Leader under PRESTO (Precursor Research for Embryonic Science and Technology, Japan) program in 2001. He was awarded by Optical Science and Technology Society for his contribution to the technology of femtosecond laser initiated nanofabrication in 2002. He received the Outstanding Young Scientist Award issued by the Ministry of Education, Culture, ports, Science and Technology, Japan, in 2006, and the Wang Daheng Optics Award issued by China Optical Society, in 2009.